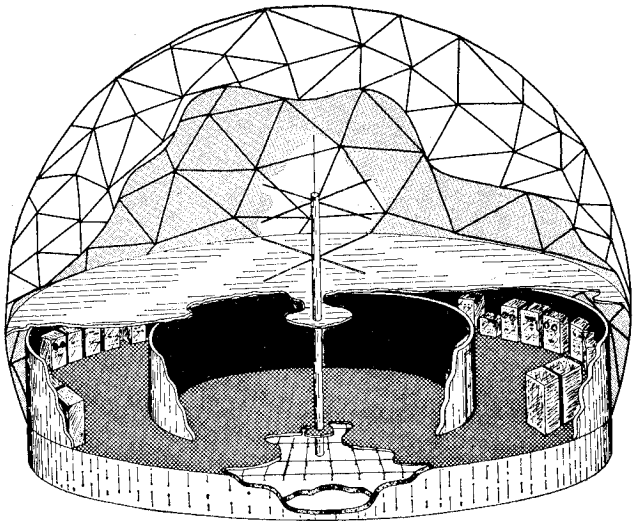

Fig. 3 Meteor trail and Nike-Met radar equipment rack layout.

last confirmed location of the target is displayed so that if the target track is lost, the operator will have the best "look" angles and range data available for reacquisition. For maximum help in acquisition, the controller can be programed prior to a rocket firing to display extrapolated look angles in real-time after the time of firing and if desired, the Nike-Met radar can be kept slewed to this extrapolated search point.

9) The Nike-Met radar is equipped with a subharmonic, pulsed transmitter and an antenna system piggy-backed and aligned with the 12-ft primary parabolic antenna with a double-the-frequency automatic frequency control (AFC) for the X-band receivers to permit the use of a two-frequency radar scheme. In this mode of operation, a pilot balloon being tracked by the radar is equipped with a 4.5 GHz harmonic generating diode in a one-half wavelength dipole wire antenna. The X-band radar transmitter is turned off, and the subharmonic transmitter emits short pulses of rf energy at 4.5 GHz. When the signal is received by the diode assembly on the balloon, it is retransmitted at twice the frequency by harmonic generation. The 9.0 GHz signal is received and tracked by the X-band Nike-Met antenna and ranging system. Since the AFC locks the receivers onto a frequency of twice the transmitter frequency, the balloon is detected at 9.0 GHz and tracked in a background free of all radar ground clutter. Tracking can occur at ranges less than those dictated by the usual recovery times of the T-R tubes (which are not used in this configuration).

The Nike-Met radar pedestals are enclosed in heated, insulated, metal space frame radomes so that all-weather maintenance and operation of the equipment can be accomplished without loss of tracking accuracy as shown in Fig. 2.

Facility Layout

The Nike-Met radar track and plot electronics racks are removed from their trailers and placed with the MTR electronics racks on a floating floor in an insulated, all dielectric radome 18 m (55 ft) in diameter as shown in Fig 3. The ceiling of the equipment room in the radome is placed at the equatorial diameter of the radome. It is made of metal faced, 4-in. polyurethane foam insulation structure board and forms the solid metal center part of the MTR counterpoise. The counterpoise, extending from the radome some 20 m (65 ft) along the radius, is composed of 15 cm (6-in.)-square electrically conducting mesh properly supported and leveled. The Nike-Met radar track pedestals in their insulated radomes are located beyond the edge of the counterpoise on a diameter through the center radome to reduce line-of-sight interference.

In areas where the sounding facility provides its own site air surveillance (such as the Alaska station) a TPS-1D surveillance radar is incorporated into the station; however, where air surveillance is provided by the range host (Fort Sherman, Canal Zone), only the MTR and the Nike-Met X-band precision tracking radars are used.

Conclusion

When installed in the summer of 1971 and completed in 1972 (funds permitting) these modified sounding facilities will provide upper atmosphere meteorological sounding support at remote sites comparable to the best missile range measurements, with a significant reduction in expenditure of material and personnel.

References

[1] Thomas, H. J. and Ward, H. P., "Study and Experimentation of RF Pulse Generating and Amplifying Techniques for Improving Radar Emission Characteristics," RD-69-33, Nov. 1969, Raytheon Co., Equipment Div., Wayland Lab.

[2] Benjamin, R., *Modulation, Resolution and Signal Processing in Radar, Sonar and Related Systems*, Pergamon Press, Oxford, 1966, p. 20.

Gravity-Induced Free Convection Effects in Melting Phenomena for Thermal Control

R. L. Bain,* F. J. Stermole,† and J. O. Golden‡
Colorado School of Mines, Golden, Colo.

Nomenclature

c_p = specific heat
d = solid-liquid interface position in y direction
k = thermal conductivity
L = length of cell in direction of long axis of cell
T = temperature
x = position in direction of long axis of cell
y = position in direction of short axis of cell, measured from the heated plate
y_0 = one-half length of cell in direction of short axis
α = angle of inclination of long axis from horizontal
ρ = density
θ = time

Subscripts

f = fusion
i = initial
l = liquid
p = hot plate
o = cold plate
s = solid

PHASE change thermal control techniques have received increasing attention, in the last several years, for spacecraft thermal design.[1–4] Because of inherent advantages of simplicity and reliability, a passive solid-liquid phase change material can be used in the walls of spacecraft as

Received January 29, 1971; revision received April 1, 1971. This work was done as a part of NASA research contract NAS8-30511, Space Sciences Laboratory, Marshall Space Flight Center, Huntsville, Ala.

* Graduate student, Chemical and Petroleum Refining Engineering Department.

† Professor, Chemical and Petroleum Refining Engineering Department.

‡ Associate Professor, Chemical and Petroleum Refining Engineering Department.

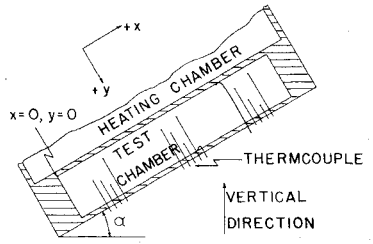

Fig. 1 Diagram of test cell.

packaging around sensitive electronic equipment to absorb or release energy to maintain constant temperature of the electronic equipment. However, this system is limited by the heat rejection or absorption capacity of the material used.

A previous study[5] has determined the property requirements of phase change materials in order that they be good thermal control devices. The material should be nontoxic, chemically inert and stable, noncorrosive, have small density variations, and a high latent heat of fusion. The material should also melt in the 50 to 150°F range; n-paraffins with an even number of carbon atoms are the most widely used materials for this purpose. In this study n-octadecane was used.

Reference 2 considered the unidimensional melting of a finite paraffin slab. It was concluded that the pure conduction model might not completely solve the phase change problem. Therefore, the present study included an investigation of the effects of gravity-induced free convection upon the melting phenomena.[6]

A two-dimensional, pure conduction model was developed in this study. The model predicted the transient temperature distribution and the solid-liquid interface profile when heat transfer was a function of thermal conduction.

The equations governing the two-dimensional problem have been developed by Carslaw and Jaeger.[7] These equations are

Solid phase

$$\partial T_s/\partial\theta = k_s/\rho_s c_{ps}(\partial^2 T_s/\partial x^2 + \partial^2 T_s/\partial y^2)$$

Liquid phase

$$\partial T_l/\partial\theta = k_l/\rho_l c_{pl}(\partial^2 T_l/\partial x^2 + \partial^2 T_l/\partial y^2)$$

The boundary conditions for the system under study were: at $y = 0$, $T = T_p$; at $y = d$, $T = T_f$; at $y = 2y_0$, $T = T_0$; at $x = 0$ and L, $T = T_p - y\ (T_p - T_0)/2y_0$; at $\theta = 0$, $T(x,y,\theta) = T_i$.

The method of excess degrees was used to predict the phase change. An explicit finite-difference method was used to approximate the equations. A Fortran-IV computer program was used to solve the equations for the theoretical temperature profiles.

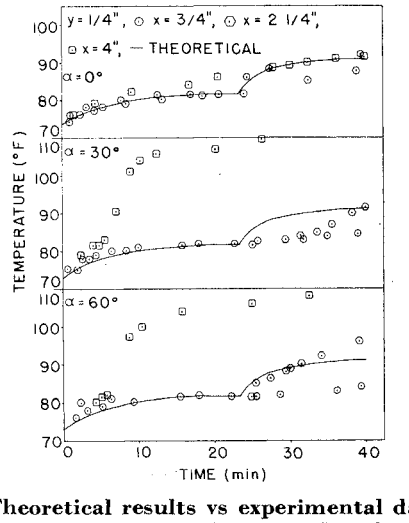

Fig. 2 Theoretical results vs experimental data for $y = \frac{1}{4}$ in. from hot plate at different angles of inclination.

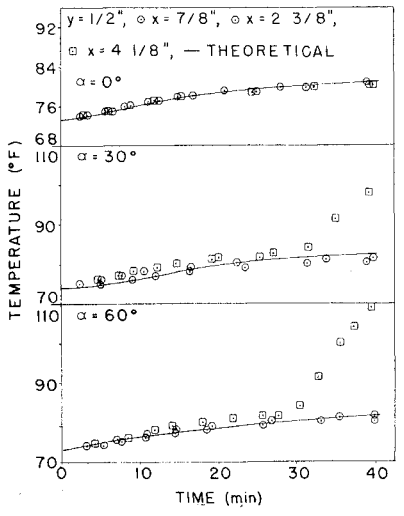

Fig. 3 Theoretical results vs experimental data for $y = \frac{1}{2}$ in. from hot plate at different angles of inclination.

The test cell, shown in Fig. 1, consisted of a rectangular test chamber, a heating chamber, and an expansion chamber (not shown in diagram). The dimensions of the test chamber were 1 in. by 5 in. by 5 in. The cell was heated by flowing heated fluid through the heating chamber. Detailed diagrams of the flow system and test cell are given in Ref. 6. Experimental temperatures were measured by means of fourteen iron-constantan thermocouples. Experimental runs were made at angles of inclination of the cell of 0°, 30°, and 60° with respect to the horizontal direction.

Partial results from the study are presented here. Figure 2 presents a comparison of theoretical profiles to experimental data for $y = \frac{1}{4}$ in. from the hot plate at 0°, 30°, and 60° angles of inclination. The spread in the results for the 0° run is due to the presence of air bubbles in the test cell. These results show, in a qualitative manner, the effects of the gravity-induced free convection, and indicate that the magnitude of the effect is a function of the angle of inclination.

Figure 3 presents theoretical and experimental results for 0°, 30°, and 60° angles of inclination at $y = \frac{1}{2}$ in. from the hot plate. The effect of convection is still present; however, during the experimental runs the magnitude of the effect is less than at $y = \frac{1}{4}$ in. because the thermocouples are further from the hot plate.

The study has demonstrated that gravity-induced free convection greatly alters the melting interface profile and the temperature profiles of individual nodes within the phase change material. The results show that the pure conduction model cannot predict these effects and that a combined conduction-convection heat transfer and fluid dynamics model must be developed.

Research is being conducted at the Colorado School of Mines under NASA sponsorship to develop a conduction-convection model to predict the effects of gravity-induced free convection upon the phase change process.

References

[1] Bannister, T. C. and Bentilla, E. W., "Study on Thermal Control by Use of Fusible Materials," *Proceedings of The Annual Technical Meeting*, Institute of Environmental Sciences, 1966, pp. 593–607.

[2] Pujado, P. R., Stermole, F. J., and Golden, J. O., "Melting of a Finite Paraffin Slab as Applied to Phase-Change Thermal Control," *Journal of Spacecraft and Rockets*, Vol. 6, No. 3, March 1969, pp. 280–284.

[3] Ukanwa, A. O., Stermole, F. J., and Golden, J. O., "Phase Change Solidification Dynamics," *Journal of Spacecraft and Rockets*, Vol. 8, No. 2, Feb. 1971, pp. 193–196.

[4] Shah, A. P., "A Microscopic and Thermal Study of the Solidification of n-octadecane," Thesis T-1334, 1970, Colorado School of Mines, Golden, Colo.

[5] Bentilla, E. W., Stewart, K. F., and Kane, L. E., Final Rept., Contract NAS8-11163, April 1966, Northrup Space Laboratories, Hawthorne, Calif.

[6] Bain, R. L., "The Effect of Gravity-Induced Free Convection Upon the Melting Phenomena of a Finite Paraffin Slab," Thesis T-1319, 1970, Colorado School of Mines, Golden, Colo.

[7] Carslaw, H. S. and Jaeger, J. C., *Conduction of Heat in Solids*, Oxford University Press, London, 1959, pp. 281–296.

Heat-Transfer Correlations for Blunt Cones at Angle of Attack

GEORGE F. WIDHOPF*
The Aerospace Corporation, San Bernardino, Calif.

THE prediction of heat-transfer rates over a blunt cone at angle of attack is a complex numerical problem at best. In any comprehensive analysis, the influence of three-dimensional effects, as well as entropy swallowing, must be included. The inclusion of either of these effects is not a trivial task. Thus, it would be useful to have an effective means of computing the surface heat transfer without the necessity of determining the detailed flow environment for every individual case. This Note presents a convenient correlation of the local heat-transfer rate with the local surface pressure for blunt cones at angles of attack. The correlation is demonstrated utilizing two sets of experimental data; one for the turbulent case and one for the laminar case.

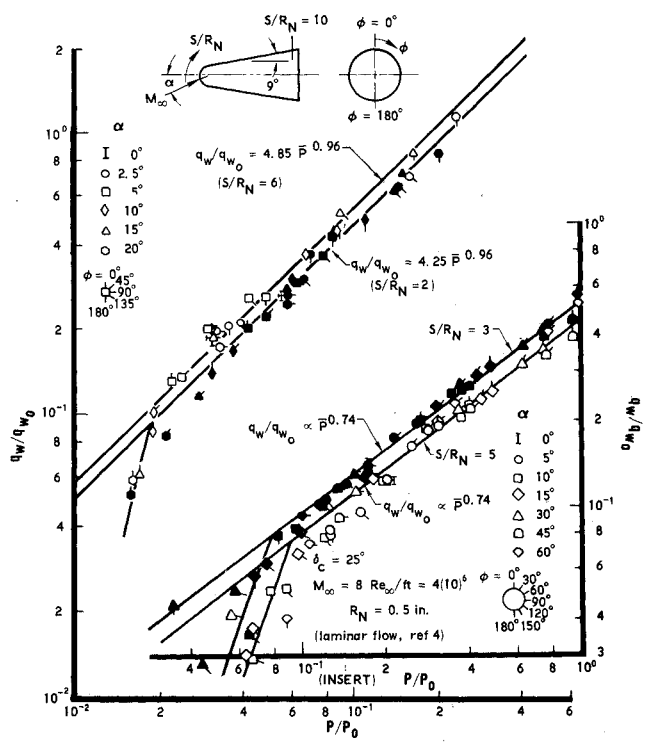

Fig. 1 Correlation of turbulent data at stations S/R_N = 2 and 6. Insert: Correlation of laminar data from Ref. 4.

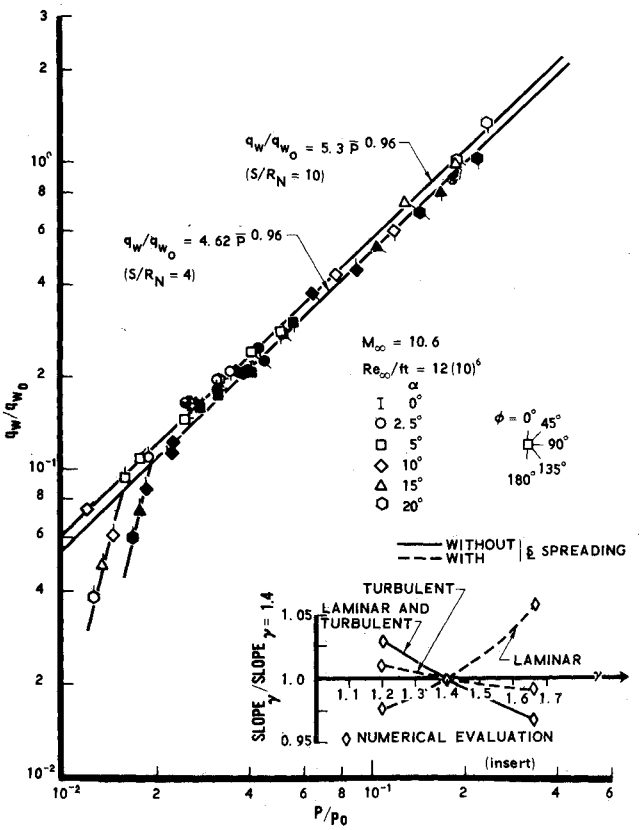

Fig. 2 Correlation of turbulent data at stations S/R_N = 4 and 10. Insert: Variation of slope with γ.

Detailed distributions of the turbulent heat-transfer rate and surface pressure measured on a blunt (R_N = 2.5 in.), 9°, half-angle cone at angles of attack of α = 0°, 2.5°, 5°, 10°, 15° and 20° were presented in Ref. 1. The measurements were made in a nitrogen environment at M_∞ = 10.6 and Re_∞/ft = 12(10)^6. There, the similarity between the heat transfer and surface pressure contours was noticed. Further analysis of the pressure and heat-transfer data was performed to determine the extent and nature of the similarity. The results, plotted in logarithmic coordinates, are shown in Figs. 1 and 2 for various locations on the conical surface measured in the angle-of-attack coordinate system depicted. Here, the local values of the turbulent heat-transfer rate nondimensionalized with respect to the measured laminar stagnation rate (q_w/q_{w_0}) are plotted against the corresponding value of the surface pressure nondimensionalized with respect to the stagnation point pressure ($p/p_0 = \bar{p}$). At each station, data corresponding to the indicated circumferential locations were plotted for each angle of attack discussed previously.

These results show that at each specific S/R_N station, the data can be correlated (within ±12%, or approximately the accuracy of the data itself) by a straight line of slope 0.96. Thus, at each station, data for various circumferential locations corresponding to various angles of attack can all be correlated by a line of a single slope over a one and one-half order of magnitude variation in pressure and heat transfer. It is also interesting to note that the data in the separated region seems to also follow a definite trend.

In Ref. 1, it was shown that the turbulent heat transfer formulation proposed by Vaglio-Laurin[2] is a good approximation in a three-dimensional environment. In those calculations, inviscid surface streamlines were traced over the cone utilizing the experimental pressure distribution, and the heat-transfer rate calculated along each streamline. Thus, the effect of streamline spreading was included in the prediction

Received April 16, 1971. The author would like to thank F. Fernandez for some helpful suggestions and comments.

* Member of the Technical Staff. Associate Member AIAA.